Journal of Catalysis **202,** 296–307 (2001)
doi:10.1006/jcat.2001.3281, available online at http://www.idealibrary.com on IDEAL®

Oxidation Reactions over RuO_2: A Comparative Study of the Reactivity of the (110) Single Crystal and Polycrystalline Surfaces

H. Madhavaram,* H. Idriss,*,[1] S. Wendt,† Y. D. Kim,† M. Knapp,† H. Over,†,[1] J. Aßmann,‡ E. Löffler,‡ and M. Muhler‡

*Centre for Surface and Materials Science, Department of Chemistry, The University of Auckland, Auckland, New Zealand; †Fritz-Haber Institut der Max-Planck Gesellschaft, Faradayweg 4-6, 14195 D-Berlin, Germany; and ‡Laboratory of Industrial Chemistry, Ruhr-Universität Bochum, D-44780 Bochum, Germany

Received January 24, 2001; revised May 13, 2001; accepted May 20, 2001; published online August 9, 2001

The present work is devoted to the investigation of oxidation reactions over RuO_2 surfaces. Two main points are addressed. First, on the fundamental level, a detailed investigation of the site requirement for CO (as well as for methanol) and O_2 adsorption on the surface of a well-defined RuO_2(110) crystal is conducted. Second, a comparison with polycrystalline RuO_2 toward these oxidation reactions is presented. Both results, those in UHV over RuO_2(110) and those at atmospheric pressure over polycrystalline RuO_2, agree fairly well. This indicates that the surface chemistry of the (110) single crystal is very similar to that of the polycrystalline material. Both the activity of the RuO_2(110) surface in the UHV regime and the activity of polycrystalline RuO_2 in the high-pressure regime were investigated by temperature-programmed desorption and by X-ray photoelectron spectroscopy. The reasons for the unusually high catalytic activity for oxidation reactions of RuO_2 are traced back to the strong bonding of the reactants over the undercoordinated Ru atoms together with the presence of weakly bound undercoordinated oxygen species, serving as the oxidizing agent.

I. INTRODUCTION

RuO_2 is now receiving considerable attention for its extraordinarily high catalytic activity (below room temperature) toward CO oxidation. This reaction was investigated at the atomic scale by applying a whole battery of surface science techniques under ultra high vacuum (UHV) conditions (1–3). To test the potential of this surface for other reactions, the present work is devoted to the investigation of the oxidation reaction of methanol over RuO_2 surfaces and compares it to CO. Considering both oxidation reactions, CO to CO_2 and methanol to formaldehyde and CO_2, as a case study, the work mainly addresses the following questions. (i) On a fundamental level, what is (are) the site requirement(s) of this very efficient oxidation reaction? In that regard, a detailed investigation of the site requirement for CO (as well as for methanol—as a representative of organic pollutants) and O_2 adsorption on the surface of a well-defined RuO_2 is analyzed. (ii) With regard to application, what is the reactivity of polycrystalline RuO_2 toward these oxidation reactions and how does it compare with UHV experiments of RuO_2 single crystal? A complementary question arises from the second one. (iii) What is the behavior of a reduced (oxygen defected) Ru oxide surface toward these same reactions? This latter point is central to our understanding of oxidation reactions over oxides in general, since ideally the surface is continuously oscillating between the oxidized and reduced states. To achieve this objective, a comparative study is conducted to investigate the reactivity of rutile RuO_2(110) single crystal, under ultra high vacuum conditions, as well as that of polycrystalline RuO_2 at 1 atmosphere, toward these oxidation reactions. This work shows that both results agree fairly well.

Rutile RuO_2(110) surface (like rutile TiO_2(110) and SnO_2(110)) possesses alternating rows of fivefold and sixfold coordinated Ru cations (the fivefold coordinated Ru cations are designated *cus*-Ru, where *cus* stands for *coordinatively unsaturated sites*. The energies of the relaxed (110) surfaces of these three oxides are relatively comparable (1.78 (4), 1.78 (5), and 2.06 (6) eV per unit cell for TiO_2(110), RuO_2(110), and SnO_2(110), respectively).

Only very recently, has detailed work been conducted under UHV conditions of the rutile RuO_2 (110) single crystal surface (3). The adsorption sites of RuO_2 for several molecules such as CO, N_2 (7), and methanol (8) are shown to be on the *cus*-Ru atoms. Two main differences are clearly observed between rutile RuO_2(110) and the corresponding surfaces of TiO_2 or SnO_2: (i) Thermal desorption spectroscopy (TDS) (1), as well as first principles density functional theory (DFT) calculations (7), has shown that unlike CO adsorption over *cus*-Ti of TiO_2(110) or *cus*-Sn of SnO_2(110), CO adsorption on *cus*-Ru is very strong (1.2 eV (7)). This is to be compared with CO-TiO_2(110) =

[1] To whom correspondence should be addressed.

0021-9517/01 $35.00

0.3 eV (4) and CO-SnO_2(110) = 0.25 eV (6). (ii) Unlike TiO_2 and SnO_2, terminal bonded atomic oxygen can be stabilized on RuO_2(110) with a binding energy of 3.1 eV (9); for comparison the bridging oxygen on RuO_2(110) is bonded by 4.6 eV (values are given with respect to neutral atomic oxygen in the gas phase). These two essential differences, the strong CO adsorption and the presence of dissociative adsorption of O_2 molecules (with high sticking probability) (10), at moderate temperatures, explain naturally the high activity of RuO_2(110) for CO oxidation (11). This high activity is unusual when compared not only to TiO_2(110) and SnO_2(110) but also, in fact, to any other known oxide single crystal to date.

The reactions of methanol and ethanol on the surfaces of oxide materials are of technological and fundamental importance (12, 13). Moreover, besides its use as a model for fundamental research, methanol is an atmospheric pollutant, with a tropospheric concentration reaching up to 5 ppbv and a relatively long lifetime (ca. 1 week) (14). It is used as a fuel additive and as such its concentration in the atmosphere is expected to rise worldwide. In addition, methanol is a good candidate, in the next decade or so, as a source for H_2 production for fuel cells. Since present fuel cell technology does not tolerate the presence of CO (formed by partial oxidation of methanol), it is thus important to rely on chemical processes completely selective for the oxidation of carbon-containing molecules to CO_2.

A detailed study of the reaction of alcohols over oxide surfaces can be found in Ref. (12). It is, however, worth mentioning a few points. Over TiO_2(110) methanol is unreactive (15). For example, DFT calculations have shown that dissociative adsorption is almost not favored on TiO_2(110) (nor on SnO_2(110)) surfaces. The adsorption energies of methanol over TiO_2(110), at $\theta = 1$ ML, is 70.4 and 74.3 kJ mol^{-1} for nondissociative and dissociative modes, respectively (15). Those on SnO_2(110) for the same modes were 110.4 and 114.5 kJ mol^{-1} (16). As will be shown in this work there is a dramatic difference between the reactivity of rutile RuO_2(110) and that of rutile TiO_2(110) toward this organic compound.

II. EXPERIMENTAL DETAILS

II.A. Polycrystalline RuO_2

Polycrystalline RuO_2 (purity >99.9%) was obtained from Merck-Schuchardt Corp. BET analysis has shown that it has a surface area of 9.8 m^2/g. TPD was performed using a fixed-bed reactor containing 30 mg of RuO_2. More details about the TPD apparatus can be found in Ref. 50.

RuO_2 is heated under O_2 for 2 h or under hydrogen for 18 h at 573 K ($P = 760$ Torr). After cooling to room temperature (under O_2 or H_2) the reactor was pumped down to 10^{-3} Torr. Methanol was placed in a saturator at room temperature. It was cleaned by freeze–pump–thaw cycles. Dosing of the reactant on the oxide was conducted by allowing the vapor pressure (ca. 100 torr) to equilibrate between the reactor and methanol, typically for 3 min. The reactor was then pumped by a roughing pump for ca. 1 h at room temperature to remove traces of the reactant in the TPD line as well as weakly adsorbed molecules on the surface of the catalyst. The gas flow was introduced into the vacuum chamber through the interface (50). The ramping rate during TPD was kept fixed at 15 K/min. The fragmentation pattern of each product was checked to identify unambiguously the reaction products by following the method described in Refs. (17, 18).

XPS analyses were performed using a KRATOS XSAM-800 model with a base pressure of ca. 10^{-9} torr. AlK_α($h\nu$ = 1486.6 eV) radiation was used at 180 W. Ar-ion sputtering experiments were performed, at room temperature, using a direct-beam KRATOS ion gun at a pressure of ca. 5×10^{-7} Torr. An accelerating voltage of 2.7 kV was used, and the emission current was 20 mA. Unreduced RuO_2 was loaded into the system without further treatment. Narrow scans were obtained with a pass energy of 20 eV, which translates to an energy resolution of 1.1 eV. In the case of H_2-reduced RuO_2 the reactor valves were closed before transferring the sample to the XPS instrument. There, the powder was transferred onto the stainless steel sample stub with indium foil, under an oxygen-free nitrogen atmosphere. The sample stub was then transferred into the vacuum chamber. The whole process of transferring the sample took 30–40 s.

XRD spectra were collected using a Phillips 1130 generator and a Phillips 1050 goniometer. Radiation by X rays was achieved using a Cu tube (broad focus) ($K_\alpha : \lambda$ = 1.514 Å) at 44 kV and 20 mA. Diffraction patterns were collected from 10° to 90° (2θ).

The temperature-programmed reduction (TPR) experiments were performed in a quartz cell built according to the design by Monti and Baiker (19) using a heating rate of 2 K/ min. Prior to the TPR measurement, RuO_2 was heated to 573 K using a heating rate of 10 K/min in synthetic air (20.5% O_2 in N_2) with a volumetric flow rate of 100 ml/min. Under these flow conditions, RuO_2 was calcined at 573 K for 2 h followed by cooling in synthetic air to room temperature. After flushing in diluted H_2 (4.2 vol% H_2 in Ar, purities 99.999%, supplied by Messer Griesheim) for 30 min, the heating ramp up to 573 K was started using a flow rate of 84.1 ml/min. The effluent gas mixture was passed through a cold trap at 195 K to remove water and analyzed quantitatively by a calibrated thermal conductivity detector (Hydros 100, 0–5% H_2 in Ar, supplied by Rosemount).

II.B. RuO_2 Single Crystal

The UHV measurements were conducted in a stainless steel chamber as described elsewhere (20). RuO_2 (110)

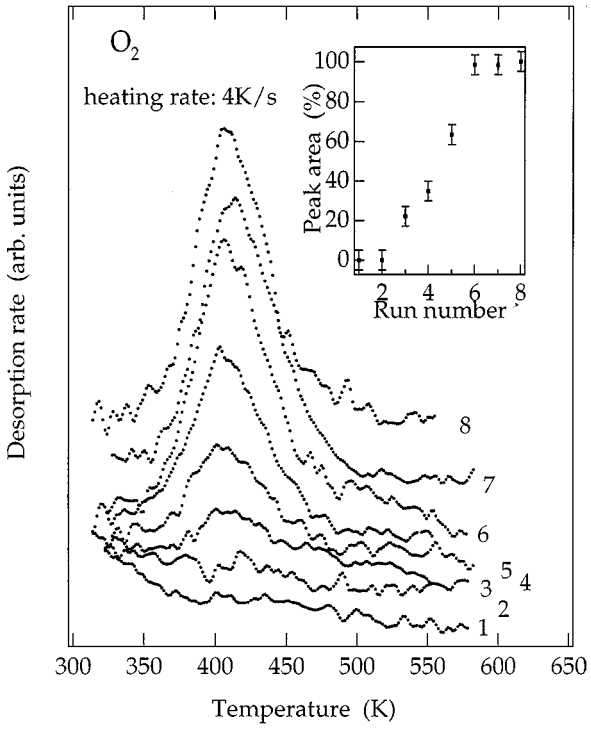

FIG. 1. Successive O_2-TPD after 0.1 L exposure over RuO_2(110) surface at 200 K. The inset shows the noncalibrated peak area of desorbing O_2 molecules as a function of dosing pressure. The *y* axis in the figure shows the noncorrected *m*/*e* 32 mass spectrometer signal.

single crystal surfaces were prepared as described in detail elsewhere (3, 21). Owing to the extreme reactivity of the surface, its stoichiometry must be checked prior to every run (or at least on a daily bases). Restoration of the surface can be achieved by successive dosing of oxygen at room temperature followed by TPD. The saturation of a TD peak at 420–430 K (previously assigned as Oγ (9) and shown as the precursor for filling in the removed bridging oxygen) indicates that surface defects have been healed. Figure 1 shows a typical sequence of desorption spectra of O_2 (*m*/*e* 32); the inset shows the peak area as a function of the number of TPD runs i.e., until saturation). Ultra pure methanol (from Aldrich) was carefully degassed by cycles of cooling with liquid nitrogen and annealing the vessel to room temperature, while continuously pumping the vapor above the frozen methanol. This procedure was iterated until no bubbles appeared during methanol melting.

III. RESULTS

III.A. Polycrystalline RuO_2

III.A.1. X-Ray Photo Emission Data

X-ray photoelectron spectra of Ru3d for O_2-annealed polycrystalline RuO_2, room temperature Ar^+-sputtered RuO_2, and high-temperature (573 K) H_2-reduced RuO_2 are presented in Fig. 2. The corresponding O(1s) to Ru(3d) ratios are given in Table 1 (also shown is the effect of Ar^+ sputtering on this ratio). The XPS Ru($3d_{5/2}$) is shown at 281.2 ± 0.1eV with a spin orbit splitting $3d_{5/2}$–$3d_{3/2}$ of 4.1 ± 0.1 eV. This spectrum is very similar to that reported in Refs. (22, 23). These line positions are those of Ru^{4+} cations (22, 23). A component at ca. 282.8 eV is also seen. This contribution is assigned in Ref. (23) to unscreened Ru^{4+} cations by comparison with the binding energy of nonmetallic Ru^{4+} oxides. In other words the line at 281.2 eV (in Fig. 2) is due to screened Ru^{4+} cations since RuO_2 is metallic (24). The full width at half maximum (FWHM) of the Ru($3d_{5/2}$) line of 2.0 eV is quite large, in particular if this value is compared to a line width of about 0.6 eV for a well-defined RuO_2(110) surface (see Section III.B.1). We interpret the large value for the FWHM of polycrystalline RuO_2(110) as originating from a inhomogeneous broadening due to the presence of several orientations of RuO_2 surfaces and the presence of defects. A clear shift is seen upon H_2 reduction (Fig. 2c) or Ar^+ sputtering (Fig. 2b). The shift of 0.7 ± 0.1 eV (XPS Ru($3d_{5/2}$) = 280.5 eV) is identical whether the surface has been reduced with H_2 or Ar^+-sputtered for 40 min. We should note that Ar^+-sputtering preferentially removes oxygen from the RuO_2 surface. The line at 280.5 eV is probably showing a large contribution from Ru metal, since Ru metal has a binding energy of 280.0–280.3 eV (Table 1) and no other stable Ru cations with oxidation state lower than +4 are known to exist in the solid state. The O(1s) emission occurs at 529.7 eV, indicative of O anions. The tail of the O(1s) peak is most likely a contribution from surface hydroxyls at ca. 532 eV (25) (Fig. 3). Also shown in the figure is the O(1s) obtained after hydrogen reduction as well as after Ar-ion sputtering. Table 1 shows that one indeed is removing O atoms by H_2 reduction, further confirming the XPS Ru(3d) results. However, the remaining presence of these XPS O(1s) lines indicates the presence of chemisorbed oxygen on and/or within the reduced material. This interpretation is supported by the observed O(1s) peak position at 530.5 eV, which is assigned to chemisorbed oxygen (Fig. 3, see Section III.B.1 for other details). We should emphasize that the bond energy of Ru–O in chemisorbed O on Ru metal is stronger by more than 1 eV than the corresponding bond of RuO_2 (9). In fact, this is why Ru metal is unusually nonreactive compared to other noble metals; once the surface is covered with O atoms, it becomes very difficult to remove them (1, 2, 26). One can measure the extent of reduction by the decrease of the O(1s) to Ru(3d) corrected peak area intensity ratios. This change can also be correlated to the FWHM of the Ru(3d) peaks since this latter decreased with increasing sputtering time. As indicated in Figs. 4 and 5 sputtering as a function of time (as well as H_2 reduction) does decrease the FWHM of Ru($3d_{5/2}$) peaks with concomitant lowering of the binding energy. Also shown is the decreasing of the O(1s)/Ru(3d) lines with

TABLE 1

XPS Binding Energy of Ru($3d_{5/2}$), O(1s), and Corrected Peak Area Ratios

Material	XPS Ru ($3d_{5/2}$) (eV)	FWHM (eV)	XPS O (1s) (eV)	Δ = (O(1s)–Ru($3d_{5/2}$)) (eV)	XPS O(1s)/Ru(3d)	Ref.
Ru/O						
Thin film	281.0		530.0	249.0		22
Ru/O						
Powder	281.9					28
RuO_2(110)						
Single crystal	280.8	0.5*	529.48	248.88		This work
	280.5		529.0	248.5		27
RuO_2(100)						
Single crystal	280.7		529.6	248.9		27
RuO_2						
Polycrystalline	281.2	2.0	529.7	248.5	1.86	This work
	280.7		529.4	248.7		24
RuO_2/Ti Electrode	280.7		529.2	248.5		25
Ar^+-sputtered RuO_2						
Polycrystalline						
5 min	280.9	1.43	530.7	249.8	0.75	This work
10 min	280.7	1.30	530.6	249.9	0.40	This work
40 min	280.6	1.26	530.5	249.9	0.40	This work
RuO_2(110)						
Single crystal[a]	279.6				0.37	27
H_2-reduced RuO_2						
Polycrystalline	280.5	1.13	530.4	249.9	0.31	This work
Ru						
Polycrystalline	280.0					24
	280.2					25
	280.3					22
Ru(0001)						
Single crystal	279.8	0.20[b]				36
Ru(0001)–(1 × 1)O	280.12[c]	0.21[b]	530.07	249.95		This work
	281.05[d]	0.39[b]	530.07	249.02		This work

[a] 0.5 kV, 15 μm/cm^2, 30 min [27].
[b] High-resolution core level shift—see experimental part for more details.
[c] Bulk Ru metal (Fig. 10).
[d] Ru three-fold coordinated to O atoms (Fig. 10).

increasing sputtering (due to preferential oxygen removal). Because of the presence of chemisorbed oxygen (together with an energy resolution of >1.1 eV), the FWHM and the position of the XPS Ru ($3d_{5/2}$) line of the hydrogen-reduced as well as the 40-min. Ar^+-ion-sputtered samples might be larger than those expected from pure Ru metal.

It does appear that H_2 reduction is at least as good as if not more efficient in reducing RuO_2 than Ar^+ sputtering

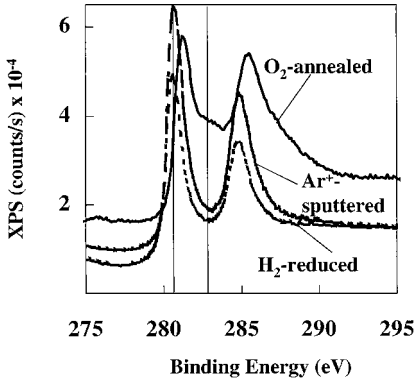

FIG. 2. XPS of the Ru(3d) region for polycrystalline RuO_2 (a), 40 min Ar^+-sputtered RuO_2 (b), and H_2-reduced RuO_2 (c).

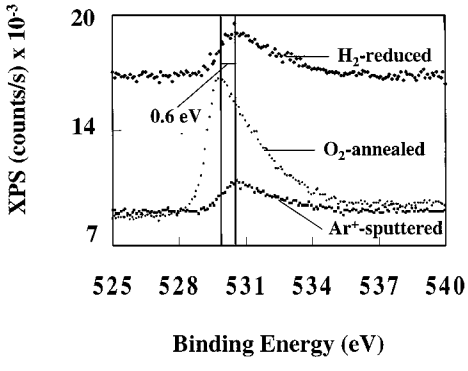

FIG. 3. XPS O(1s) of O_2-annealed RuO_2 (a), 40 min Ar^+- sputtered RuO_2 (b), and H_2-reduced RuO_2 (c).

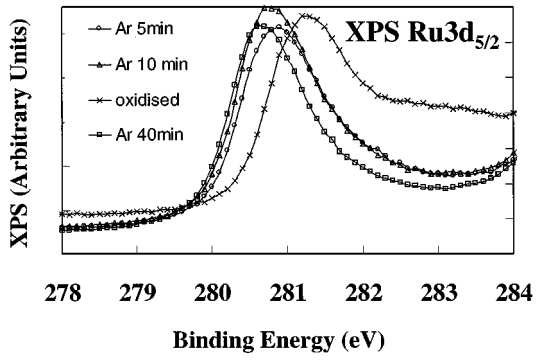

FIG. 4. XPS of the $Ru(3d_{5/2})$ region of polycrystalline RuO_2 as a function of sputtering time with Ar ions; all other conditions are kept constant. (a) 5 min Ar^+-sputtered RuO_2, (b) 10 min Ar^+-sputtered RuO_2, (c) 40 min Ar^+-sputtered RuO_2, and (d) H_2-reduced RuO_2.

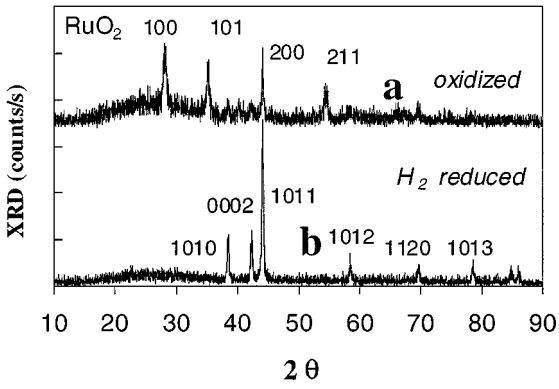

FIG. 6. XRD of (a) O_2-annealed (573 K, 1 atm) and (b) H_2-reduced (573 K, 1 atm) polycrystalline RuO_2.

(see the values of both Δ and O(1s)/Ru(3d) in Table 1). This is by no means universal, as H_2 reduction usually has a marginal effect when compared to Ar^+ sputtering for most oxide materials. For example, H_2 is thought to adsorb only on defect sites of TiO_2(110) surface, with an isosteric heat of adsorption of 83 $kJmol^{-1}$ (29) while no evidence for its adsorption is found on the fully oxidized Ti foil (30). However, Ar-ion sputtering may reduce up to 75% of the Ti^{4+} cations into $Ti^{x+}(x < 4)$ of single crystal or polycrystalline TiO_2 surfaces (31, 32).

III.A.2. X-Ray Diffraction Data

The effect of the extent of reduction was also monitored by XRD. XRD did indicate that indeed a bulk transformation occurs because RuO_2 has been transformed to Ru metal by H_2 reduction. The spectra compare well with those found in the literature (33–35). They are also consistent with XPS Ru(3d) lines and may strongly indicate that the amount of oxygen (about 20%) observed by XPS can be assigned to chemisorbed or dissolved oxygen on and/or in metallic Ru (Fig. 6).

III.A.3. Temperature-Programmed Reduction of RuO_2

Figure 7 displays two TPR profiles obtained by using sample weights of 102.4 mg and 26.6 mg. Calculating the constant P defined as $P = \beta S_0/Fc_0$ according to Malet and Caballero (36) yields values of 9.8 and 2.5 K, respectively, where β is the heating rate, S_0 is the amount of reducible species, and Fc_0 is the molar H_2 flow rate into the reactor. Values of P lower than 20 K were found to be appropriate to obtain good peak resolution (36). Accordingly, a narrow TPR peak with a full width at half maximum of 20 K (solid curve) was obtained. The sharp onset of reduction below 390 K indicates an autocatalytic process triggered by the formation of metallic Ru nuclei providing atomic hydrogen. Both the peak position at 391 K and the low FWHM are in good agreement with the TPR results obtained by Hurst

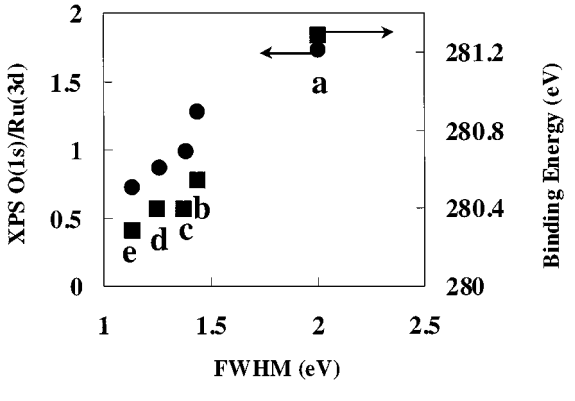

FIG. 5. Corrected peak area ratios of XPS O(1s) to XPS Ru(3d) of polycrystalline RuO_2 (a), 5 min Ar^+-sputtered RuO_2 (b), 10 min Ar^+-sputtered RuO_2 (c), 40 min Ar^+-sputtered RuO_2 (d), and H_2-reduced RuO_2 (e) as a function of the FWHM of the corresponding XPS $Ru(3d_{5/2})$ (x-axis). Also shown is the corresponding binding energy position of $Ru(3d_{5/2})$ (right hand side of y-axis).

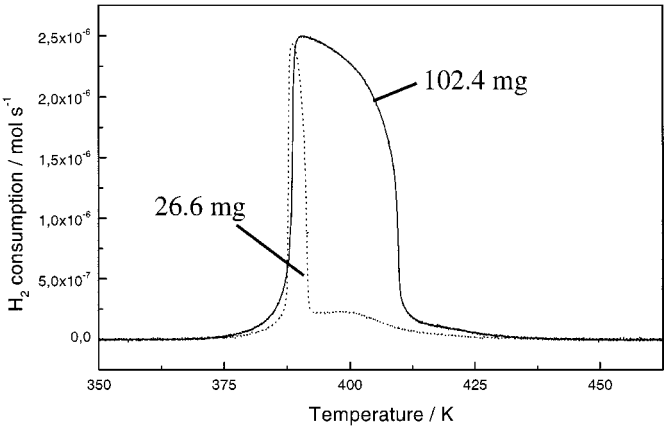

FIG. 7. TPR of polycrystalline RuO_2. (Solid line) Sample weight, 102.4 mg; (dotted line) sample weight, 26.6 mg. Heating rate, 2 K/s.

et al. (37). Decreasing S_0 by a factor of 4 yields an even higher resolution (dotted curve). This TPR profile consists of a very narrow peak at 388 K and a broader peak at 398 K. The latter may originate from an inhibiting influence of water on the reduction kinetics.

The degree of reduction was calculated based on the following equation:

$$RuO_2 + 2H_2 \rightarrow Ru + 2H_2O. \qquad [1]$$

Averaging the amount of H_2 consumed in six TPR experiments yields a value of 99.7%, which indicates full reduction to metallic Ru within the experimental accuracy. The presence of polycrystalline metallic Ru at the end of the TPR was also confirmed by XRD.

III.A.4. Temperature-Programmed Reactions over RuO_2

Figure 8 shows TPD after methanol adsorption at room temperature over polycrystalline RuO_2. Formaldehyde (*m/e* 29, 30), methyl formate (*m/e* 60), CO (*m/e* 28), CO_2 (*m/e* 44), H_2 (*m/e* 2), and water (*m/e* 18) were observed, in addition to unreacted methanol (*m/e* 31) (Table 2). All primary alcohols have their strongest signal at 31 *m/e* due to CH_2OH^+ species. It is more accurate to consider the *m/e* 31 signal for quantitative analysis rather than the parent molecule because of its high intensity. This is particularly important in the case of methanol when TPD is conducted at pressure above ca. 10^{-8} Torr because its parent molecule (*m/e* 32) interferes with O_2 from the background. Quantitative analyses were computed following the methods described in Refs. (17, 18), where the major fragmentation patterns (up to 5) of each product were accounted for. Products desorbed in three temperature domains. The first (below 390 K) consisted of methanol, formaldehyde, methyl formate, H_2O, and H_2. As summarized in Table 2 these desorptions combined contributed 2.7% of the overall carbon products. In Fig. 8 H_2 is shown to desorb at a slightly higher temperature than formaldehyde (about 10 K). Several runs were conducted addressing this particular observation. H_2 desorption temperature was seen either exactly at the formaldehyde peak temperature or shifted by up to 10 K higher (as seen in Fig. 8). The shift was not consistent from one run to the other. It is most likely that cooling the reactor under O_2 had an effect on the state of the RuO_2 surface. A stabilization effect due to surface oxygen on the recombinative desorption of H_2 where surface O atoms have indeed delayed D_2 desorption over U metal has been observed by other workers (38). Since the experiments were conducted over RuO_2 that has been cleaned with O_2 at 573 K and cooled under O_2 to 300 K before evacuation, it is not unreasonable to consider that some weakly held oxygen left on the surface retards the recombination of H atoms.

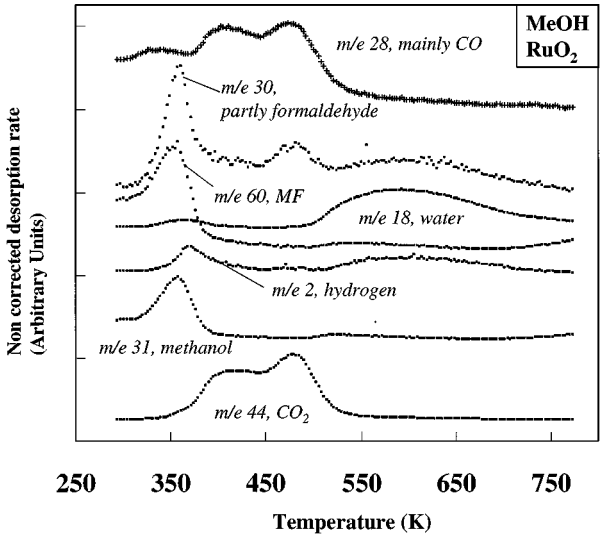

FIG. 8. TPD after methanol adsorption at 300 K over polycrystalline RuO_2. RuO_2 has been O_2-annealed at 573 K (1 atm) and cooled under O_2 to 300 K.

TABLE 2

Carbon Yield and Peak Temperature of Products Resulting from TPD after Methanol Adsorption over Polycrystalline RuO_2 at 300 K

Reactant/product	Temperature (K)	Carbon yield (%)
Methanol (*m/e* 31)	360	1.72
Formaldehyde (*m/e* 30)	360 and 480	0.44
Methyl formate (*m/e* 60)	360	0.58
CO_2 (*m/e* 44)	410 and 480	87.66
CO (*m/e* 28)	410 and 480	9.59
H_2 (*m/e* 2)	370, 480, >520	—
H_2O (*m/e* 18)	>520	—

The second desorption domain (380–520 K) mainly consisted of CO and CO_2 with some formaldehyde and H_2. This latter desorption contributed over 97% of the total carbon products. The third desorption domain (510–750 K) contained H_2O with some H_2. No carbon-containing products are observed in this temperature region with the probable exception of some formaldehyde.

Three main points are worth noting. (i) Almost all adsorbed methanol (saturation coverage) has reacted, as evidenced by a desorption of only 1.7% of the initial amount (the surface was exposed to 18×10^3 torr of methanol prior to TPD). (ii) The total decomposition mainly gave CO_2 (a CO_2/CO of ca. 9), indicating that oxygen anions are easily removed from the surface. (iii) Some formaldehyde (*m/e* 30) is left (0.44%) and some has reacted via Tishchenko reaction (ester formation) to give methyl formate (0.58%) (see Refs. 12 and 13 for more details on this reaction).

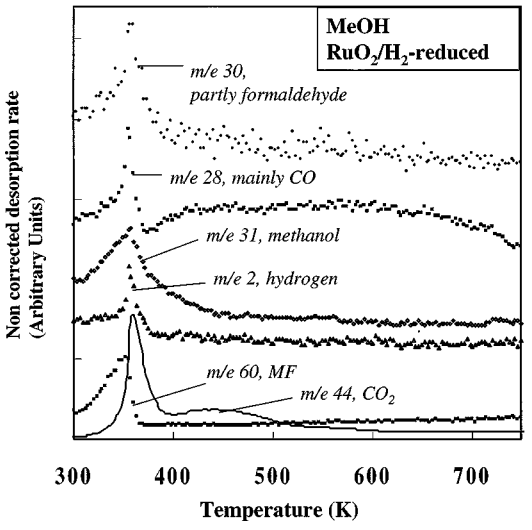

FIG. 9. TPD after methanol adsorption at 300 K over H_2-reduced RuO_2 (573 K, 1 atm).

III.A.5. Temperature-Programmed Reactions over Reduced RuO_2

TPD measurements of methanol over H_2-reduced RuO_2 were also conducted. Considerable differences in the product distribution are observed (Fig. 9 and Table 3). First, all products desorbed at lower temperatures. Second, an early CO_2 desorption is clearly seen with a peak at 360 K. Both the 360 and 450 K desorption contributed 50% of the desorption products. CO desorption accompanied the low-temperature CO_2 peak and contributed ca. 11% of the carbon yield. Formaldehyde, which was observed in trace amounts on the stoichiometric surface, has increased severalfold, accounting for 20% of the overall products. Similarly, methyl formate desorption has increased ca. 20 times (11.5%). Because formaldehyde is most likely a reaction intermediate to CO_2 formation, it is not unexpected to observe an incomplete oxidation on the reduced RuO_2 surface (see Scheme A [2–4] below, where (a) is adsorbed, (s) is surface, V_O is oxygen vacancy, (g) is gas). Moreover, the increase of methyl formate may simply be explained as due to the high concentration of formaldehyde (Scheme B) because 2 mol of formaldehyde may react, giving 1 mol of methyl formate (Tishchenko reaction).

TABLE 3

Carbon Yield and Peak Temperature of Products Resulting from TPD after Methanol Adsorption at 300 K over H_2-Reduced (at 573 K, 1 atm, Cooled under H_2 to 300 K) Polycrystalline RuO_2

Reactant/product	Temperature (K)	Carbon yield (%)
Methanol (*m/e* 31)	360	6.82
Formaldehyde (*m/e* 30)	360	20.63
Methyl formate (*m/e* 60)	360	11.25
CO_2 (*m/e* 44)	360 and 450	49.97
CO (*m/e* 28)	360 and >400	11.32
H_2 (*m/e* 2)	360	—
H_2O (*m/e* 18)	370	—

Scheme A

$$CH_3OH + O\ (s) \rightarrow CH_3O\ (a) + OH\ (a) \quad \text{OH dissociation} \quad [2]$$

$$CH_3O\ (a) \rightarrow CH_2O\ (g) + H(a) \quad \text{Dehydrogenation} \quad [3]$$

$$H(a) + OH\ (a) \rightarrow H_2O\ (g) \quad \text{Water removal} \quad [4]$$

$$CH_2O\ (a) + 2O\ (s) \rightarrow CO_2\ (g) + H_2O\ (g) \quad \text{Decomposition} \quad [5]$$

$$CH_2O + O\ (s) \rightarrow CO\ (g) + H_2O\ (g) \quad \text{Decomposition} \quad [6]$$

Scheme B

$$2CH_2O\ (a) \rightarrow HC(O)OCH_3\ (g) \quad [7]$$

Yields in Tables 2 and 3 are carbon-based and not molar-based. In other words about 1/3 of the formaldehyde left is forming methyl formate (assuming no other reaction of the latter).

III.B. UHV Experiments

III.B.1. X-Ray Photo Emission Data of Ru(0001)–(1 × 1)O and RuO_2(110) Single Crystals

High-resolution core level shift (HRCLS) experiments of a well-defined RuO_2(110) surface in comparison with the Ru(0001)–(1 × 1)O were performed at the beamline I311 at MAXII in Lund, Sweden (39). The photon energies used were $h\nu = 380$ eV and 680 eV for Ru(3d) and O(1s), respectively. The energy resolutions of the Ru($3d_{5/2}$) and O(1s) spectra were set to 80 MeV and 180 MeV, respectively (to be compared with the 1.1 eV in the polycrystalline experiments). The HRCL spectra of Ru($3d_{5/2}$) and O(1s) were taken at 100 K and are depicted in Fig. 10. For the Ru(0001)–(1 × 1)O surface clearly two well-resolved Ru($3d_{5/2}$) peaks are visible; these are assigned to bulk Ru (280.12 eV, FWHM: 0.21 eV) and Ru coordinated to three oxygen atoms in the surface layer (281.05 eV, FWHM: 0.39 eV). The corresponding O(1s) photoemission line is at 530.07 eV (FWHM: 0.55 eV) (Fig. 10a; see also Table 1). $\Delta_1 = (O(1s)–Ru(3d_{5/2}))$ (where Ru($3d_{5/2}$) is at 280.12 eV) is equal to 249.95 eV. This value is very close to that obtained for polycrystalline oxide that has been Ar-ion sputtered or H_2-reduced (249.8–249.9).

Upon oxidation of the Ru(0001)–(1 × 1)O surface, as detailed in Section II, as well as in Refs. (3, 21, 39), RuO_2(110) is formed. Its surface was also analyzed (Fig. 10b). There is a major change in both the Ru and O regions. The Ru($3d_{5/2}$ peak is now at about 280.8 eV, but a component at 280.2 eV can still be present (it is worth recalling that LEED (21) and STM (3) have shown the coexistence of Ru(0001)–O(1 × 1) with RuO_2(110)). The small component at 280.2 eV is thus due to the contribution from Ru metal atoms in Ru(0001)–O(1 × 1) phase. The shift to lower binding energy of the

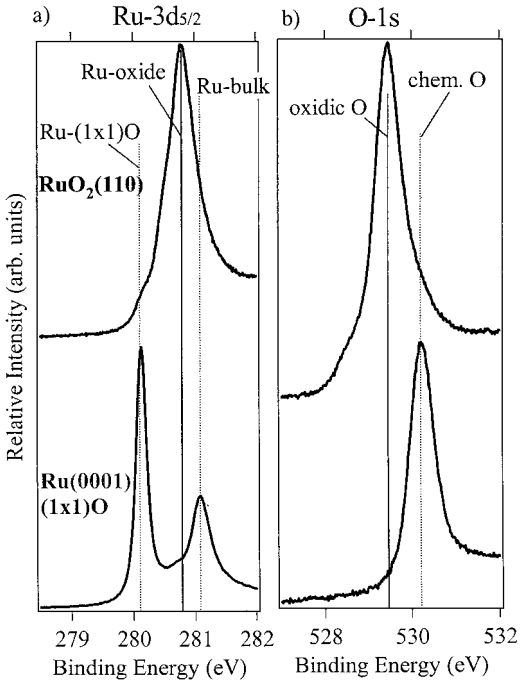

FIG. 10. HRCLS spectra of $Ru3d_{5/2}$ and O(1s) for (a) Ru(0001)–(1 × 1) O single crystal and (b) RuO_2(110) single crystal.

O(1s) (from 530.07 to 529.48 eV) together with that of the main Ru atoms to higher binding energy (from 280.12 to 280.8 eV) contributing to $\Delta_1 = (O(1s)–Ru(3d_{5/2})) =$ 248.88 eV is very close to that observed on polycrystalline materials (Table 1).

III.B.2. CO and O_2 Reactions over RuO_2(110) Single Crystal

i. LEED spot intensity measurements. Oxygen exposure to the clean RuO_2(110) surface leads to the stabilization of a weakly held oxygen species that desorbs with a peak at 420 K (see Fig. 1). This weakly held oxygen has been shown to adsorb over *cus*-Ru atoms (9). The weakly held oxygen serves as a precursor state to heal the missing bridging oxygen atoms of the RuO_2(110) surface. This behavior is clarified in Fig. 11, in which the spot intensity of a RuO_2(110) related LEED beam is shown as a function of the CO exposure (as well as O_2 exposure) at a sample temperature of 520 K. With increasing CO exposure the LEED intensity decreased; a change in slope is observed at about 90 L. Oxygen postexposure was able to recover a large part of the original LEED intensity signal. A saturation is reached after an O_2 exposure of 80 L. The main point to make from this figure is that the oxidation–reduction cycle of this oxide single crystal surface can be conducted and monitored under mild conditions (low temperatures and relatively low exposures). To completely restore the LEED signal a more prolonged exposure to O_2 or several O_2-TPD runs, as shown in Fig. 1, are required.

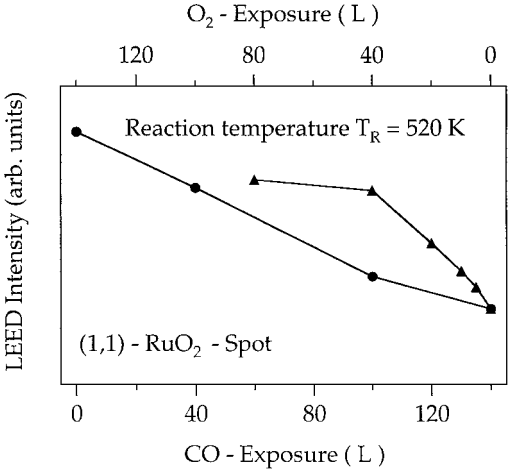

FIG. 11. LEED spot intensity (1, 1) of RuO_2(110) single crystal that has been subjected to increasing CO exposure followed by O_2 treatment.

ii. Temperature-programmed reaction of CO over RuO_2(110). Successive CO-TPD experiments (after CO exposure at 170 K) were conducted over stoichiometric RuO_2(110)—as the starting material, but without regeneration with O_2 molecules in between runs. The amount of CO_2 produced decreased with successive runs upon a cumulative exposure of 2.5 L, down to below the detection limits of the QMS (Fig. 12a). This is due to removal of available surface oxygen (most likely the twofold bridging oxygen atoms; see Section IV). This behavior is in fact observed only if the ramping stops just after CO and CO_2 desorptions have taken place (450 K). In contrast, if CO-TPD runs are conducted up to elevated

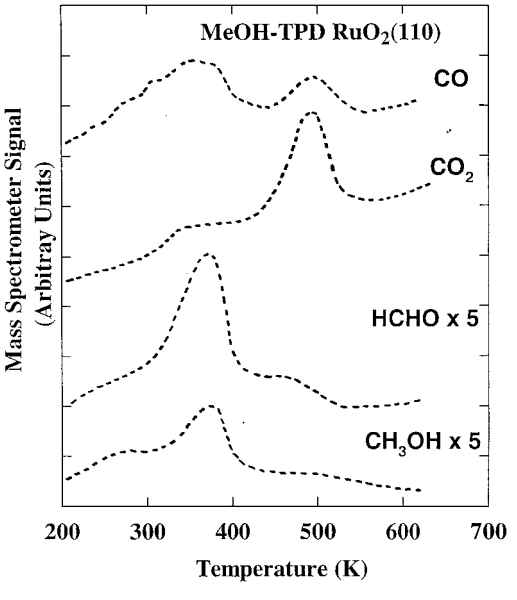

FIG. 12. TPD after methanol adsorption (2 L) over RuO_2(110) single crystal surface at 200 K.

temperatures, a different TPD profile is observed (Fig. 12b). In this latter situation postdosing of CO (at 293 K) results in a gradual increase of peak areas of desorbed CO_2. Saturation is achieved by ca. 570 K. This latter observation provides clear evidence of self-regeneration of the active sites due to a temperature effect. Comparison with STM pictures, collected under similar conditions (3), indicates that this behavior may be associated with oxygen migration from the threefold sites to the twofold (bridging) sites (see Section IV). In other words, this behavior is not necessarily due to bulk to surface diffusion of lattice oxygen.

iii. Temperature-programmed reaction of methanol over RuO_2(110). In Fig. 13 we present the thermal desorption data after the clean RuO_2(110) surface has been exposed to 2.4 L methanol at 200 K. The main product (ca. 70%) leaving the surface after a rise in the sample temperature is CO_2. The main peak appears at ca. 480 K and is accompanied by a small peak at 380 K. These peak positions compare favorably with those of the high-pressure experiments (Fig. 8). CO desorption took place at the same temperatures (380 and 480 K) but with a different distribution. The low-temperature desorption was about twice as large as the high-temperature desorption (see Table 4 for quantitative analysis). The similarity with Fig. 8 is easily noticed. Methanol desorption takes place at 380 K. Most of the formaldehyde leaves the surface at 380 K (a large peak) although a small desorption at 500 K is also observed. Both methanol and formaldehyde desorptions appear at the same position as those observed in the high-pressure work (compare Figs. 8 and 13).

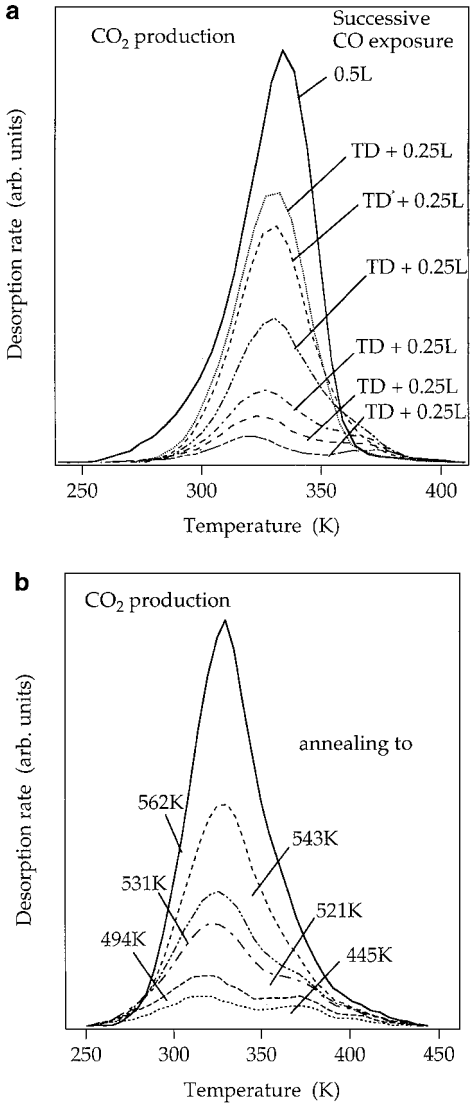

FIG. 13. Successive TPD after CO adsorption over RuO_2(110) single crystal surface without (a) and with (b) surface regeneration; regeneration was conducted by heating the surface to the indicated temperature.

TABLE 4

Carbon Yield and Peak Temperature of Products Resulting from TPD after Methanol Adsorption (2 L) over Stoichiometric RuO_2(110) Single Crystal at 200 K

Reactant/product	Temperature (K)	Carbon yield (%)
CH_3OH (m/e 31)	390	13.0
HCHO (m/e 30)	390	24.2
CO_2 (m/e 44)	385	13.0
	485	27.2
CO (m/e 28)	385	15.4
	485	7.2
CO_2/CO		1.78
CO_2 + HCHO		64.4

IV. DISCUSSION

Several main points resulting from the above study are worth mentioning.

1. Ru cations in polycrystalline RuO_2 can be easily reduced (either by H_2 or upon Ar^+sputtering) as evidenced by a shift of the XPS Ru($3d_{5/2}$) line by 0.7 eV (from 281.2 to 280.5 eV) (Fig. 2). This shift is consistent with that observed by HRCLS from model surfaces of Ru(0001)–(1 × 1)O and RuO_2(110) single crystals (from 281.05 to 280.05 eV) (Fig. 10).

2. One can measure the shift as a Δ, where Δ = XPS O(1s) − XPS Ru($3d_{5/2}$). Δ was equal to 248.88 and 248.5 eV for RuO_2 single crystal and polycrystalline materials, respectively. On the reduced (either by H_2 or by Ar^+ bombardment) RuO_2 polycrystalline surface Δ = 249.9 eV, which is identical to that of Ru(0001)–(1×1)O single crystal (Δ = 249.95 eV) (Table 1).

3. XRD (Fig. 6) as well as TPR (Fig. 7) has indicated that H_2-reduced polycrystalline RuO_2 has been bulk transformed to Ru metal. Although the O(1s) to Ru(3d) peak-area ratios decreased dramatically (Figs. 4 and 5), the

TABLE 5

Formaldehyde Yield during Methanol-TPD over Several Oxide Single Crystals and Computed Activation Energies of Formaldehyde Desorption

Oxide single crystals	Yield (%)	Peak temperature (K)	Activation energy[f] (kcal/mol)	References
Rutile TiO_2(110)[a]	0	—		45
Cubic ZrO_2(100)[b]	0	—		43
Rocksalt MgO(100)[c]	0	—		47
Wurtzite ZnO(0001)-Zn[d]	1–2	520	32 (0.03–0.06)[g]	40
Rutile TiO_2(001)-{011}	4	640	40 (0.1)	41
Fluorite CeO_2(111) thin film	—[h]	560–580	35–36	44
Rutile SnO_2(110)[e]	10–20	450	28 (0.36–0.72)	42
Cubic ZrO_2(110)	15	450	28 (0.54)	43
Rutile RuO_2(11)	24	390	24 (1)	This work

[a] Molecular adsorption at room temperature, UPS data; no other products were observed.
[b] Other products included CH_4 and CO.
[c] Dissociative adsorption, XPS data; no other products were observed.
[d] Peak areas and yield were computed from Fig. 1 in Ref. 40.
[e] Given value = 11%. Variations from run to run put a yield value between 10 and 20% (42).
[f] Estimated by Redhead analysis, assuming first-order pre-exponential factor (10^{13} s^{-1}) (49).
[g] Yield (%)/activation energy (kcal/mol).
[h] Quantitative analyses were not provided; formaldehyde formation was highly sensitive to prior annealing conditions (44).

residual presence of O atoms at binding energy higher than that of O(1s) in RuO_2, together with the absence of the RuO_2 phase in XRD, suggests the formation of some dissolved or chemisorbed oxygen on metallic Ru. The shift in the XPS O(1s) peak position to higher binding energy (Fig. 3 and Table 1) is also indicative of chemisorbed oxygen atoms.

4. The surface of RuO_2(110) could be regenerated by dosing O_2 molecules (<1 L, direct dosing) at room temperature (Fig. 1).

5. The self-regeneration of the active centers for CO oxidation to CO_2 was clearly shown to occur when one heats the RuO_2(110) to 570 K and above.

6. Both polycrystalline RuO_2 and RuO_2(110) surfaces behaved similarly toward methanol oxidation to formaldehyde, as well as toward its total decomposition to CO and CO_2 (Figs. 8 and 13).

In addition to the above six points, results from previous and parallel works (1–3, 7, 8) have indicated that CO adsorption occurs preferentially on *cus*-Ru (DFT calculation (7, 8), STM (3)). Similarly, LEED-*IV* analyses have suggested that methanol adsorption occurs also on these same sites (8).

Points 1 to 4 indicate one single conclusion. It is a simple task to make reduction-oxidation cycles on RuO_2 single crystal and polycrystalline surfaces using H_2 or CO as reducing agents and O_2 as the oxidizing agent.

RuO_2(110) single crystal is unique for its activity toward CO to CO_2 and as such no comparison can be made to other oxides. However, its reactivity toward methanol oxidation to formaldehyde can be compared to that of other oxides single crystals such as ZnO (0001)–Zn (40), TiO_2(001)-{011} faceted (41), SnO_2(110) (42), ZrO_2(110) (43), and CeO_2(111) (44) single crystals. TiO_2(110) (45), MgO(100) (46), and ZrO_2(100) (43) single crystals showed no activity toward methanol oxidation to formaldehyde. Interestingly all these oxide single crystals have surface cations with at least one coordinative unsaturation. Table 5 shows the TPD yield, the peak temperature, and a computed activation energy of formaldehyde desorption for these oxides together with those of RuO_2(110) single crystal. RuO_2 is indeed more active than the other oxides. One may estimate the efficiency of the reaction by dividing the reaction yield (%) by the activation energy (or peak temperature). The higher the number, the more active the surface. These numbers were found as low as 0.03 mol/kcal for ZnO(0001)–Zn and rose to 1 mol/kcal for RuO_2(110) single crystal. Equally important, the other two rutile oxides with a (110) surface orientation are not active (see also Table 5). In other words, the coordinative unsaturation is not the sole requirement for making the oxidation. Other surface properties enter into consideration and these are discussed below.

We have asked three questions in the introduction and we attempt to answer them with the help of this study below.

Since RuO_2(110) is very active toward adsorption as well as oxidation reactions, the difference from the other oxides must lie somewhere else. It has been demonstrated that CO oxidation obeys the Mars–van Krevelen mechanism (3), where the undercoordinated surface oxygen anions (bridging oxygen anions) are consumed as a result of their reaction with adsorbed CO making CO_2. The surface defects created

that way are regenerated by gas-phase oxygen adsorption. In other words, there are at least three requirements for the reaction to occur.

(a) An active lattice oxygen must be available to react with adsorbed CO (such as the undercoordinated bridging and terminal bonded oxygen atoms).

(b) Strong adsorption sites for the reactant must be present.

(c) There must be an efficient dissociative adsorption of O_2 molecules to regenerate lattice oxygen ions.

Requirement (a) has been clearly shown in this study by the following:

(i) Adsorption of CO on RuO_2(110) single crystal gives large amounts of CO_2. This amount decreases with successive runs (on the nonregenerated surface) until its disappearance. Yet, it can be easily switched back by simply flashing the surface to 570 K (lattice oxygen migration to the active sites) (Fig. 13).

(ii) Comparing the methanol TPD runs over the stoichiometric and the H_2-reduced polycrystalline RuO_2, we observe that the amount of CO_2 decreased by almost 50% and that of formaldehyde (the partial oxidation product) increased to 20% of the product yield (Table 3).

Requirement (b) is indeed fulfilled. As mentioned in the introduction, the adsorption energy of CO over *cus*-Ru in the rutile RuO_2(110) structure (1.2 eV (3)) is ca. 4 and 5 times stronger than the corresponding adsorption over *cus*-Ti of TiO_2(110) or *cus*-Sn of SnO_2(110), respectively. A weak adsorption will result in an easy displacement of the reactant by other reactant/products (such as water) and the surface becomes nonreactive, particularly if the oxidation process is to occur at low temperatures. Requirement (c) is also met on RuO_2. Dosing O_2 molecules followed by flashing the surface to ca. 600 K (to remove on-top oxygen) over RuO_2(110) single crystal (Fig. 1) fully restored the surface. This is also evidenced by LEED spot intensity measurements (Fig. 11).

One of the intriguing results of this present study is that temperature-programmed reactions under UHV (single crystal) and high-pressure conditions (polycrystalline samples) are virtually identical. This also means that the reaction pathways are very much alike and therefore the active centers on RuO_2 are the same. Moreover, we also know that the efficiency for CO oxidation does not depend very much on the orientation of RuO_2 (47), at least not when we compare the (110), (100), and (101) orientations—all three surfaces contain *cus*-Ru. We conclude from this observation that the presence of *cus*-Ru atoms is an important requirement for the high activity of RuO_2. The (110), (100), and (101) surfaces of RuO_2 are low-energy surfaces that should equally be the prevailing orientations found on polycrystalline RuO_2.

The binding energies of bridging O and on-top O were computed to be 4.6 and 3.1 eV, respectively (values are given with respect to neutral atomic oxygen in the gas phase (9). Therefore one would expect that the CO oxidation reaction would start by consuming the on-top O species first and then the bridging O species. This has been shown in recent HREELS experiments (48). It was observed that the intensity of on-top O species has decreased with CO exposure at room temperature (i.e., reacted with CO to give CO_2). Once all on-top O atoms have been removed, the intensity of the signal from bridging O atoms decreased. When all the available bridging oxygen atoms were consumed (complete disappearance of their signal), the CO oxidation reaction stopped. This result can be compared to those of Fig. 13, where CO oxidation stops when the available surface oxygen atoms are consumed.

In summary, this work has shown that detailed analysis of a well-defined surface can shed light on a complex reaction such as CO or methanol oxidation, over a polycrystalline oxide. The fact that RuO_2 is metallic, and thus allows extensive LEED and electron spectroscopy studies, together with its unusually high activity toward oxygen and CO adsorptions and reactions has been of tremendous help in comparing the activity of a well-defined surface of RuO_2(110) to that of the polycrystalline material.

REFERENCES

1. Böttcher, A., Niehus, H., Schwegmann, S., Over, H., and Ertl, G., *J. Phys. Chem. B* **101**, 11185 (1997).
2. Böttcher, A., Rogozia, M., Niehus, H., Over, H., and Ertl, G., *J. Phys. Chem. B* **103**, 6267 (1999).
3. Over, H., Kim, Y. D., Seitsonen, A. P., Wendt, S., Lundgren, E., Schmid, M., Varga, P., Morgante, A., and Ertl, G., *Science* **287**, 1474 (2000).
4. Casarin, M., Maccato, C., and Vittadini, A., *J. Phys. Chem. B* **102**, 10745 (1998).
5. Kim, Y. D., Schwegmann, S., Seitsonen, A. P., and Over, H., *J. Phys. Chem. B* **105**, 2205 (2001).
6. Melle-Franco, M., and Pacchioni, G., *Surf. Sci.* **461**, 54 (2000).
7. Kim, Y. D., Seitsonen, A. P., and Over, H., *Phys. Rev. B* **6311**(11), 5419 (2001).
8. Kim, Y. D., and Over, H., unpublished LEED analysis.
9. Kim, Y. D., Seitsonen, A. P., Wendt, S., Wang, J., Fan, C., Jacobi, K., Over, H., and Ertl, G., *J. Phys. Chem. B* **105**, 3752 (2001).
10. Böttcher, A., and Niehus, H., *Phys. Rev. B* **60**, 14396 (1999).
11. Kim, Y. D., Over, H., Krabbes, G., and Ertl, G., *Top. Catal.* **14**, 95 (2001).
12. Idriss, H., and Barteau, M. A., *Adv. Catal.* **45**, 261 (2000).
13. Idriss, H., and Seebauer, E. G., *Catal. Lett.* **66**, 139 (2000).
14. Goldan, P. D., Kuster, W. C., and Fehenfeld, F. C., *J. Geophy. Res.* **102**, 6315 (1997).
15. Bates, S. P., Kresse, G., and Gillan, M., *Surf. Sci.* **409**, 336 (1998).
16. Calatayud, M., Andrés, J., and Beltrán, A., *Surf. Sci.* **430**, 213 (1999).
17. Ko, E. I., Benziger, J. B., and Madix, R. J., *J. Catal.* **62**, 264 (1980).
18. Idriss, H., Kim, K. S., and Barteau, M. A., *J. Catal.* **139**, 119 (1993).
19. Monti D. A. M., and Baiker, A., *J. Catal.* **83**, 323 (1983).
20. Over, H., Bludau, H., Skottke-Klein, M., Moritz, W., and Ertl, G., *Phys. Rev. B* **46**, 4360 (1992).
21. Kim, Y. D., Seitsonen, A. P., and Over, H., *Surf. Sci.* **465**, 1 (2000).

22. Chan, H. Y. H., Takoudis, C. G., and Weaver, M. J., *J. Catal.* **172**, 336 (1997).
23. Cox, P. A., Goodenough Cox, J. B., Tavener, P. J., Telles D., and Edgell, R. G., *J. Solid State. Chem.* **62**, 360 (1986).
24. Kim, K. S., and Winograd, N., *J. Catal.* **35**, 66 (1974).
25. Kötz, R., Lewerenz, H. J., and Stucki, S. **130**, 825 (1983).
26. Zhang, C. J., Hu, P., and Alavi, A., *J. Am. Chem. Soc.* 1212, 7931 (1999).
27. Atanasoska, L. J., O'Grady, W. E., Atanasoski, R. T., and Pollak, F. H., *Surf. Sci.* **202**, 142 (1988).
28. Shen, J. Y., Adnot, A., and Kaliagine, S., *Appl. Surf. Sci.* **51**, 47 (1991).
29. Göpel, W., Rocker, G., and Feierabend, R., *Phys. Rev. B.* **28**, 3427 (1983).
30. Raup G. B., and Dumesic, J. A., *J. Phys. Chem.* **89**, 5240 (1985).
31. Idriss, H., and Barteau, M. A., *Catal. Lett.* **26**, 123 (1994).
32. Reztova, T., Chang, C.-H., Koresh, J., and Idriss, H., *J. Catal.* **185**, 223 (1999).
33. Cotton F. A., and Mague, J. T., *Inorg. Chem.* **5**, 317 (1966).
34. Rogers, D. B., Shannon, R. D., Sleight, A. W., and Gillson, J. L., *Inorg. Chem.* **8**, 841 (1969).
35. Lele, S., and Anantharaman, T. R., *Acta Cryst.* A**24**, 654 (1968).
36. Malet, P., and Caballero, A., *J. Chem. Soc., Faraday Trans. 1* **84** , 2369 (1988).
37. Hurst, N. W., Gentry, S. J., Jones, A., and McNicol, B. D., *Catal. Rev.—Sci. Eng.* **24**, 233 (1982).
38. Lloyd, J. A., Manner, W. L., and Paffett, M. T., manuscript in review.
39. Over, H., Seitsonen, A. P., Lundgren, E., Wiklund, M., and Andersen, J. N., *Phys. Rev. Lett.*, submitted.
40. Vohs, J. M., and Barteau, M. A., *Surf. Sci.* **176**, 91 (1986).
41. Kim, K. S., and Barteau, M. A., *Surf. Sci.* **223**, 13 (1989).
42. Gercher, V. A., Cox, D. F., and Themlin, J-M., *Surf. Sci.* **306**, 279 (1994).
43. Dilara P. A., and Vohs, J. M, *Surf. Sci.* **321**, 8 (1994).
44. Siokou, A., and Nix, R. M., *J. Phys. Chem. B* **103**, 6984 (1999).
45. Onishi, H., Aruga, T., Egawa, C., and Iwasawa, Y., *Surf. Sci.* **193**, 33 (1988).
46. Peng, X. D., and Barteau, M. A., *Langmuir* **7** 1426 (1991).
47. Over, H., Gierer, M., Bludau, H., Ertl, G., and Tong, S. Y., *Surf. Sci.* **314**, 243 (1994).
48. Fan, C., Wang, J., Jacobi, K., and Ertl, G., *J. Chem. Phys.* **114**, 10058 (2001).
49. Redhead, P. A., *Vacuum* **12**, 203 (1962).
50. Madhavaram, H., and Idriss, H., *J. Catal.* **184**, 533 (1999).